Thin Solid Films 542 (2013) 108–113

Contents lists available at SciVerse ScienceDirect

Thin Solid Films

journal homepage: www.elsevier.com/locate/tsf

Hydrothermal–galvanic couple synthesis of directionally oriented $BaTiO_3$ thin films on TiN-coated substrates ☆

Chia-Jung Yang [a], Di-You Tsai [a], Pei-Hsuan Chan [a], Chu-Tsun Wu [b], Fu-Hsing Lu [a,*]

[a] Department of Materials Science and Engineering, National Chung Hsing University, Taichung 402, Taiwan
[b] Department of Mechanical Engineering, National United University, Miaoli 36003, Taiwan

ARTICLE INFO

Article history:
Received 4 February 2013
Received in revised form 10 June 2013
Accepted 21 June 2013
Available online 29 June 2013

Keywords:
Barium titanate
Titanium nitride
Thin films
Hydrothermal synthesis
Galvanic couple
Growth kinetics

ABSTRACT

$BaTiO_3$ films were synthesized on TiN-coated Si substrate below 100 °C by a hydrothermal–galvanic couple technique in barium contained alkaline solutions. X-ray diffraction and electron backscatter diffraction results show that the $BaTiO_3$ thin films were directionally oriented grown on the TiN/Si substrates, i.e., (111) $BaTiO_3$ over (111) TiN. The surface morphologies revealed that $BaTiO_3$ nucleated and grew over the TiN surface with a single layer. From kinetic analyses, the growth rates of $BaTiO_3$ films prepared by the hydrothermal–galvanic couple technique were faster than a hydrothermal method. The galvanic effects were confirmed by investigating the induced currents and energies. The galvanic currents were generated and controlled by both the dissolution of TiN and the formation of $BaTiO_3$. The output electric energies increased rapidly with the reaction time and leveled off at the full coverage of $BaTiO_3$.

1. Introduction

Barium titanate ($BaTiO_3$) is one of the most important electroceramic materials due to its superior dielectric and ferroelectric properties [1,2]. $BaTiO_3$ films have been widely used in cutting-edge applications, such as dynamic random access memory, chemical sensors, and multilayer chip capacitors [3–5]. In the literature, various techniques have been reported for the synthesis of $BaTiO_3$ films including pulsed laser deposition [6], ion-beam sputtering technique [7], sol–gel process [8], hydrothermal [9–16], and hydrothermal–electrochemical methods [17–25]. Most of the techniques require temperatures higher than 500 °C to enhance crystallinity of the films except hydrothermal and hydrothermal–electrochemical methods which may bring the temperature down near or below 100 °C [13–19]. Fig. 1 summarizes the lowest reaction temperature of the hydrothermal and hydrothermal–electrochemical synthesis of $BaTiO_3$ films, reported from the literature including our previous work on the hydrothermal–galvanic couple (HT–GC) and hydrothermal (HT) synthesis of $BaTiO_3$ films [26–28]. This technique can reduce the reaction temperature down even below 55 °C.

As reported in our previous work, synthesis of $BaTiO_3$ films by a HT–GC technique may significantly enhance the growth rates of the films. During the galvanic couple setup, no external power supply was required but the growth of $BaTiO_3$ films could be enhanced significantly by the induced current/voltage. Moreover, unlike the conventionally used bulk Ti, Ti/Si, or TiO_2 substrates [29–34], TiN/Si substrates were used during the synthesis of $BaTiO_3$. Because of the low resistivity and highly preferred orientation of TiN, $BaTiO_3$ films were found to grow directionally over the TiN/Si substrates [26]. Nevertheless, the growth kinetics of synthesizing the films by the HT–GC technique has not yet been investigated. The galvanic effects during the synthesis of the films have not yet been explored, either.

Thus, this work was aimed to investigate the growth kinetics of $BaTiO_3$ films synthesized by the HT–GC method and then to compare the results with those made by the sole hydrothermal method. The effect of the galvanic couple setup on the growth of the films has also been explored.

2. Experiment

TiN films were prepared on n-type (100) silicon substrates by DC reactive sputtering, as reported in our previous work [28]. The deposition time was 3 min and the resulting thickness of TiN was 400 nm. The resistivity of the obtained TiN was in the range of 310–350 μΩ cm.

In the HT–GC synthesis, the reaction solution was a mixture of 0.5 M $Ba(CH_3COO)_2$ (99.5%, J.T. Baker, U.S.A) and 2 M NaOH (99%, Riedel-de Haën, Germany) alkaline solutions. The reaction temperatures were kept below 100 °C and hence, no autoclave was required. As for the

* Corresponding author. Tel.: +886 4 22851455; fax: +886 4 22857017.
E-mail address: fhlu@nchu.edu.tw (F.-H. Lu).

0040-6090/$ – see front matter © 2013 The Authors. Published by Elsevier B.V. All rights reserved.
http://dx.doi.org/10.1016/j.tsf.2013.06.060

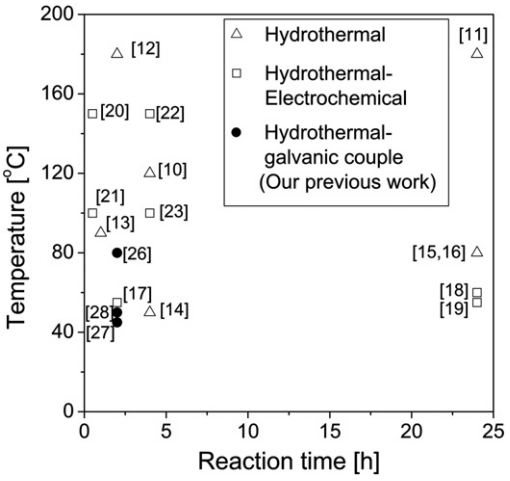

Fig. 1. The lowest reaction temperatures of the hydrothermal and hydrothermal–electrochemical synthesis of $BaTiO_3$ films, reported from the literature including our previous work [26–28].

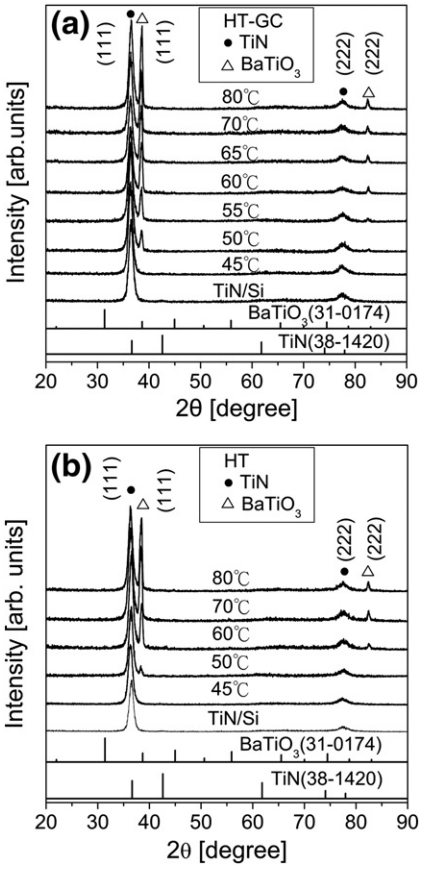

Fig. 2. X-ray diffraction patterns of $BaTiO_3$ over TiN/Si synthesized by the (a) HT–GC and (b) HT methods at various temperatures for 2 h.

galvanic couple setup, the working electrode was the TiN/Si specimens and the counter electrode was Pt while the two electrodes were directly connected without applying any external power sources.

Crystalline phases of the films were determined by X-ray diffraction (XRD) (MPX3, Mac Science, Japan) operated at 40 kV and 30 mA with a Cu Kα excitation source ($\lambda_{Cu,K\alpha} = 0.1542$ nm). Surface and cross-sectional morphologies of the films were investigated by field-emission scanning electron microscopy (FE-SEM) (JSM-6700 F, JEOL, Japan) operated at 3 kV to minimize the charging effect. Electron backscatter diffraction (EBSD) (JSM-7001 F, JEOL, Japan) was also conducted to examine the grain orientations of the obtained films. The growth kinetics was evaluated by analyzing the coverage of $BaTiO_3$ over the TiN films as a function of the reaction time. The coverage of $BaTiO_3$ was calculated by averaging five selected areas in the SEM micrographs taken from each specimen.

3. Results and discussion

3.1. Crystallinity

Fig. 2 shows the X-ray diffraction patterns of the as-deposited films and those after the (a) HT–GC and (b) HT syntheses at various temperatures for 2 h. The as-deposited films were rock-salt structured TiN (JCPDS 38-1420) [35] with a highly (111) preferred orientation. As shown in the figure, the crystalline cubic $BaTiO_3$ (JCPDS 31-0174) [35] phase was present after the syntheses at the temperatures above 50 °C and grew directionally over TiN-coated substrates. It is noteworthy that the relative intensities of $BaTiO_3$ obtained in this referenced HT synthesis were slightly different from those reported in our previous work [28]. This is mainly due to the different batch of the specimens, which doesn't affect the conclusions deduced from this work. The directionally oriented growth of $BaTiO_3$ during the HT–GC synthesis, i.e., (111) $BaTiO_3$ over (111) TiN, is also very similar to that for the HT synthesis.

3.2. Morphology

In Fig. 3, the as-deposited TiN seeding layer revealed a nano-grained structure and $BaTiO_3$ started to nucleate and grow over the seeding layer for both the (a) HT–GC and (b) HT synthesis. As shown, only a few $BaTiO_3$ particles grew over the TiN surface at 45 °C. The coverage of $BaTiO_3$ increased rapidly with the reaction temperature ranging from 45 °C to 60 °C. At reaction temperatures higher than 60 °C, the $BaTiO_3$ particles almost covered the whole TiN surface. The trend is similar to those synthesized by both the HT–GC and HT methods. At a fixed reaction temperature, the amount of $BaTiO_3$ particles obtained by using the HT–GC was obviously larger than that synthesized by the HT method in the temperature range of 45 °C—60 °C. It clearly indicates that the galvanic couple setup can facilitate the growth of $BaTiO_3$. Here, it also demonstrates that the HT–GC technique can be used to produce $BaTiO_3$ films at lower reaction temperature (<50 °C), compared to the HT and hydrothermal–electrochemical methods, as revealed in Fig. 1.

The cross-sectional view of the $BaTiO_3$ films obtained by the HT–GC method is given in Fig. 4. As-deposited TiN exhibited a characteristic columnar structure. The TiN films were then slightly consumed after the syntheses at various temperatures for 2 h. The $BaTiO_3$ particles were produced, yielding a single layer over the TiN film surface. That's why the coverage instead of thickness was used for analyzing the kinetics. It is noteworthy that the interface between TiN and formed $BaTiO_3$ was rather smooth. Moreover, porosity existed in the $BaTiO_3$ films. The porosity of the $BaTiO_3$ films can be calculated based on the theoretical estimation [36] and experimental observations. Taking the synthesis at 80 °C shown in Fig. 4 as an example, the consumed thickness of TiN was 19 ± 1 nm that should yield 64 ± 1 nm (3.4 times) of a fully dense $BaTiO_3$ film. However, the experimentally observed thickness of $BaTiO_3$ was 71 ± 1 nm. That means the porosity existing in the $BaTiO_3$ film might be about 10%. The discrepancy between the estimation and the observation may also stem from the densities used in the calculation since the bulk and film densities are possibly different and only the former value is available at the moment.

As mentioned earlier in the XRD analysis, directionally-oriented growth of the $BaTiO_3$ films was observed over the TiN seeding layer that exhibited a strong preferred orientation. To further examine the oriented growth, EBSD was also preformed over different grains

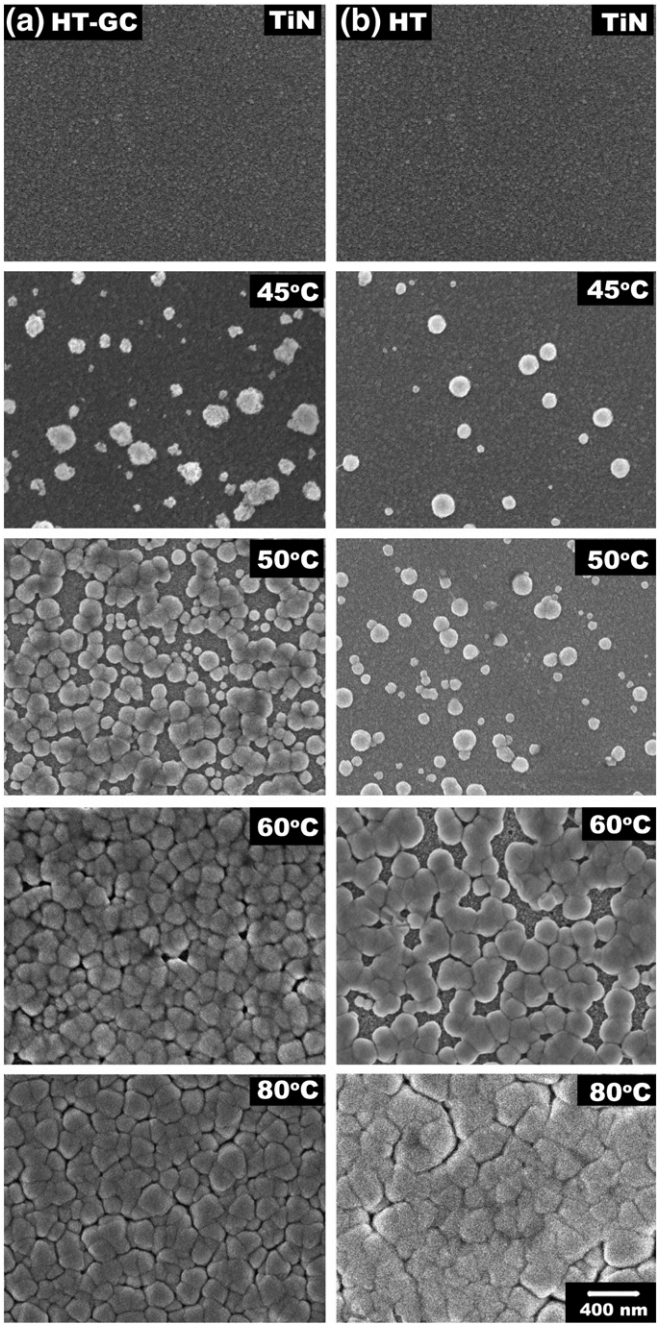

Fig. 3. FE-SEM micrographs of surface morphology of $BaTiO_3$ synthesized by the (a) HT–GC and (b) HT methods at various temperatures for 2 h.

of the obtained films. A typical set of micrographs is given in Fig. 5. Fig. 5a revealed the grains of the films selected for the electron backscatter diffraction.

From the obtained Kikuchi pattern of each $BaTiO_3$ grain, as shown in Fig. 5b, the pole figure of the different grains could be acquired, as sketched in Fig. 5c. The central point represented the [111] orientation. The other three points referred to the family of the {111} orientations. All the grains show similar results, which indicated the [111] preferred growth direction. This verified the directionally oriented growth of the oxide films, i.e., (111) $BaTiO_3$/(111) TiN. This indicates that the highly oriented TiN films can be used to design different directionally-oriented $BaTiO_3$ films by this synthesizing method. That can be also extended to other similar perovskite oxide/conductive nitride systems.

3.3. Growth kinetics

To more accurately quantify the growth kinetics of $BaTiO_3$ over the TiN seeding layer, the coverage of $BaTiO_3$, y, was fitted to a modified Avrami–Erofe'ev equation [37–40], as given below:

$$y = 1 - \exp[-k(t - t_0)]^n \quad (1)$$

where k is the rate constant, t is the reaction time, t_0 is the incubation time before the formation of $BaTiO_3$, and n is the time exponent constant. Since the coverage of $BaTiO_3$ seemed to proceed by the increase in numbers of nuclei rather than their growth, as shown in Fig. 3, such nucleation and growth behavior of $BaTiO_3$ has not been reported in the literature. Nevertheless, the Avrami–Erofe'ev or modified equation has been applied to a wide range of studies, including time-dependence of the nucleation [41], crystallization and phase transformation in glasses and alloys, metal hydrogenation reactions [42], and anion exchange reactions in layered materials [43]. Hence, a modified Avrami–Erofe'ev equation has been tried to analyze the growth kinetics. It turns out that kinetic behavior of the HT–GC and HT syntheses can be fitted rather well by the equation, as shown in Fig. 6. It indicates that the growth of the films increased quickly with the reaction time and followed the kinetic model. At fixed reaction time and reaction temperature, the coverage of $BaTiO_3$ synthesized by the HT–GC method was much larger than that prepared by HT synthesis. The growth did not occur until the reaction time exceeded the incubation time, t_0. The incubation time decreased rapidly with the temperature. As the reaction temperature increased from 50 °C to 80 °C, the incubation time was reduced from 1800 s to 50 s, for the HT–GC synthesis. Apparently higher temperatures can provide energy to overcome the potential barrier and activate the formation of $BaTiO_3$ particles. Moreover, the galvanic couple setup can also aide significantly the growth of $BaTiO_3$.

Beside the variation of the incubation time t_0 with the reaction temperatures, as sketched in Fig. 7a, other fitting parameters including n

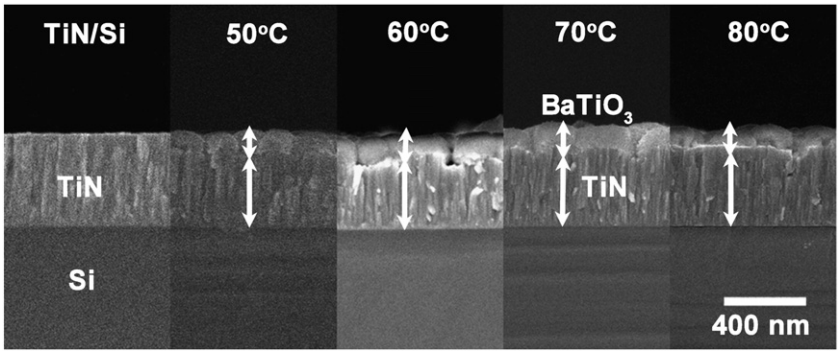

Fig. 4. Cross-sectional view of $BaTiO_3$ over TiN/Si synthesized by the HT–GC method at various temperatures for 2 h.

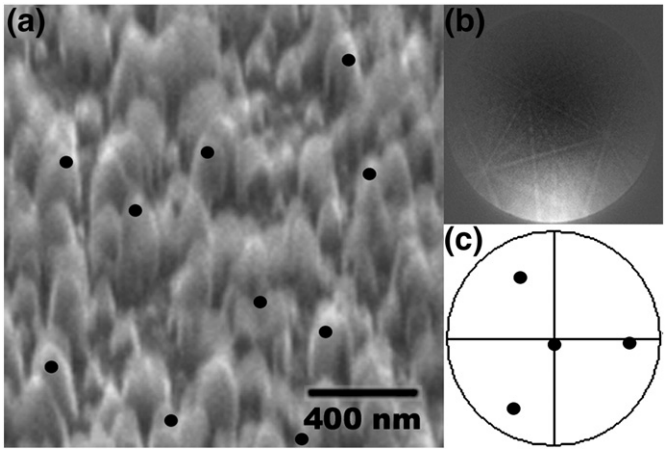

Fig. 5. (a) The tiled (70°) FE-SEM micrographs of $BaTiO_3$ after the HT–GC synthesis at 80 °C for 10 min. (b) The typical Kikuchi pattern of a selected grain designated in (a). (c)The pole figure of the selected grains indicating the [111] growth direction.

and k are shown in Fig. 7b and c. The value of n is associated with the reaction mechanism, which has been discussed in the literatures [34]. As shown in Fig. 7b, the n-value was close to 1 during the HT synthesis and was consistent with our previous work [28], which implies that the growth of films was controlled by phase boundary reactions [34]. As for the HT–GC synthesis, the n-value was also near 1 in the range of 60 °C − 70 °C. Nevertheless, the n-value was higher than 1 at the reaction temperatures below 60 °C, implying that the HT–GC synthesis might be controlled by more complex reactions. Fig. 7c shows the reaction constant k in logarithm scale against the temperature. The k-values for the HT–GC synthesis were larger than those for the HT synthesis and the difference increased with the temperature, which is apparently due to the galvanic effect during the HT–GC synthesis. This indicates that the galvanic effect during the HT–GC synthesis was more and more evident at higher temperatures and could then enhance the reaction.

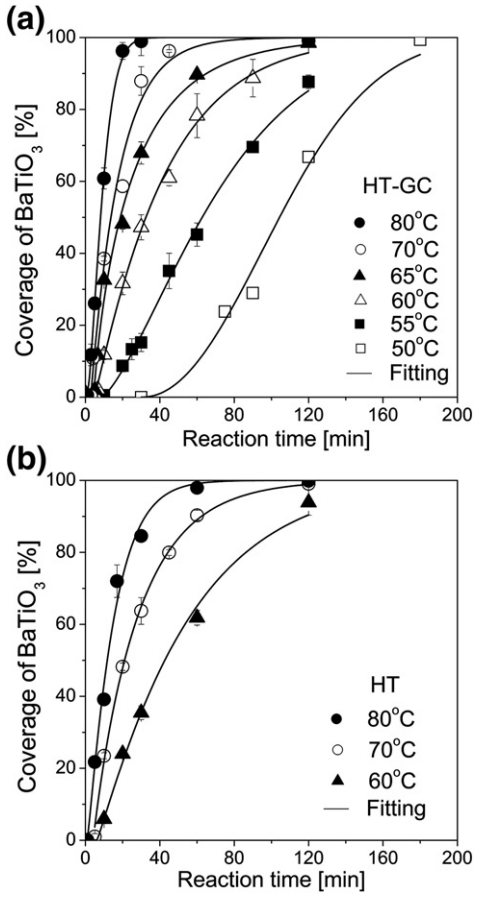

Fig. 6. The coverage of $BaTiO_3$ synthesized by the (a) HT–GC and (b) HT methods as a function of the reaction time at various reaction temperatures. The solid lines are the fitting curves by using a modified Avrami–Erofe'ev equation.

The activation energy of forming $BaTiO_3$ could be determined by fitting the rate constant to the Arrhenius-type equation.

$$k = k_0 \exp\left(-\frac{Q}{RT}\right) \tag{2}$$

where k_0 is the pre-exponent constant, Q is the activation energy, R is the gas constant, and T is the reaction temperature. From the fitting results, the calculated activation energy for the HT synthesis was 55 ± 4 kJ mol^{-1} in the temperature range of 60 °C − 80 °C, which is consistent with that reported in our previous work [28]. Nevertheless, $\ln k$ vs. $1/T$ for the HT–GC synthesis shows a nonlinear behavior. It indicates that the HT–GC technique is governed by multiple formation mechanisms including at least hydrothermal reaction and galvanic-aided formation. To explore the galvanic couple effects during the HT–GC synthesis, the induced currents and corresponding electric energies were investigated and reported in the later section.

3.4. Galvanic couple effect

It is generally recognized that HT synthesis of $BaTiO_3$ is governed by a dissolution–precipitation mechanism [44–47]. It has been reported that TiN would be oxidized in highly concentrated alkaline solutions [48]:

$$TiN + 2OH^- + H_2O \rightarrow HTiO_3^- + NH_3 + e^- \tag{3}$$

Barium ions could then react with $HTiO_3^-$ ions to form barium titanate,

$$Ba^{2+} + HTiO_3^- \rightarrow BaTiO_3 + H^+ \tag{4}$$

Since TiN exhibits a certain degree of ionic bonding in addition to covalent bonding, it may be much easier to dissolve into alkaline solutions than Ti to yield $BaTiO_3$ films, as described in our previous work for the low-temperature HT synthesis [28]. As given in Eq. (3), more enhanced dissolution reactions at higher reaction temperatures would produce more electric charges and then enhance the galvanic effects. Nucleation of $BaTiO_3$ occurred via the dissolution–precipitation mechanism. TiN firstly dissolved in alkaline solutions to form $HTiO_3^-$ ions and then reacted with Ba^{2+} ions to $BaTiO_3$. Because the TiN films exhibited nanogranular and columnar structure, as shown in Fig. 4, the dissolution of TiN in alkaline solution might occur at the grain boundaries which could accumulate high concentration of $HTiO_3^-$ ions. This may yield inhomogeneous nucleation of $BaTiO_3$.

In an electrochemical system, the current is determined by the reaction rates at the electrodes. As the electrochemical reaction occurs at the electrode–electrolyte interface, it is called heterogeneous reaction and the reaction rate depends on various factors, such as mass transfer to the electrode and electron transfer at the electrode surface. The reaction rate associated with the current density can be expressed by the following equation [49]:

$$\text{Rate}\left(\text{mols}^{-1}\text{cm}^{-2}\right) = \frac{j}{nF} \tag{5}$$

with j the current density, n the stoichiometric number of electrons in the electrode reaction, and F the Faraday constant. As shown in Fig. 8, the in-situ measured (a) current densities and (b) corresponding electric energies are plotted against the reaction time at various synthesizing temperatures. The competitive reactions of both dissolution of

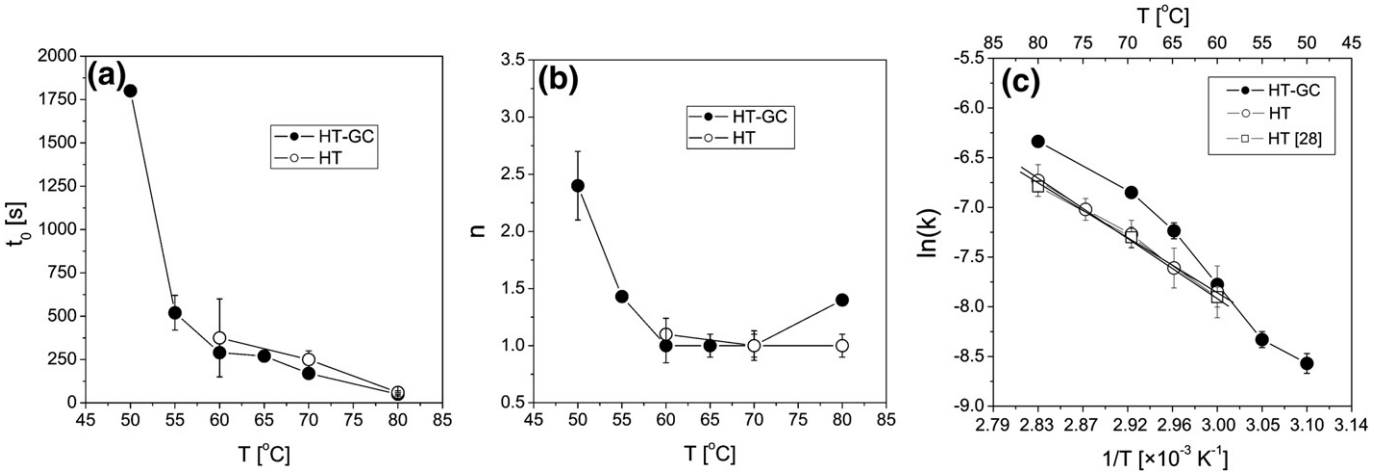

Fig. 7. (a) The incubation time t_0, (b) the time exponent constant n, versus the reaction temperature and (c) the logarithm k vs. 1/T for both the HT and HT–GC syntheses.

TiN and the formation of $BaTiO_3$ yield a maximum current density at each reaction temperature. As shown in Fig. 8a, the maximum current density increased with reaction temperatures. Higher reaction temperatures apparently enhance both reactions, causing higher maximum current density. The galvanic currents can be divided into three regimes for a fixed reaction temperature. Initially, the galvanic currents abruptly decreased to a minimum. Subsequently, the currents increased rapidly to a maximum and finally returned to a background value. It is possible that at the beginning TiN films dissolve into alkaline solution and produce $HTiO_3^-$ ions accumulated on the TiN surface, which may hinder the dissolution reaction and cause the current decrease. This time period at which $BaTiO_3$ has not yet been formed can be referred to the incubation time, as mentioned earlier. Next, the significant galvanic current increase is mainly due to the reactions of Ba^{2+} ions with $HTiO_3^-$ ions, leading to the formation of $BaTiO_3$ and further dissolution of TiN. The latter reaction results in the current increase. In our case, the dissolution of TiN and the precipitation of $BaTiO_3$ occurred concurrently at the working electrode, as given in Eqs. (3) and (4). Current density was enhanced by the dissolution of TiN while was suppressed by the precipitation of $BaTiO_3$. It is noteworthy that the maximum current density occurs at the time when half of the TiN surface was covered by $BaTiO_3$. Subsequently, the produced $BaTiO_3$ particles gradually cover over the TiN film surface and reduce the effective reaction area of the TiN films, which would hinder the dissolution of TiN and then slowly suppressed the galvanic current. After reaching full coverage of the $BaTiO_3$ particles, the galvanic effect is ceased and the galvanic current then returns to the background value. Since no external voltages or currents were applied to the system, the spontaneous currents clearly stem from the galvanic couple effect.

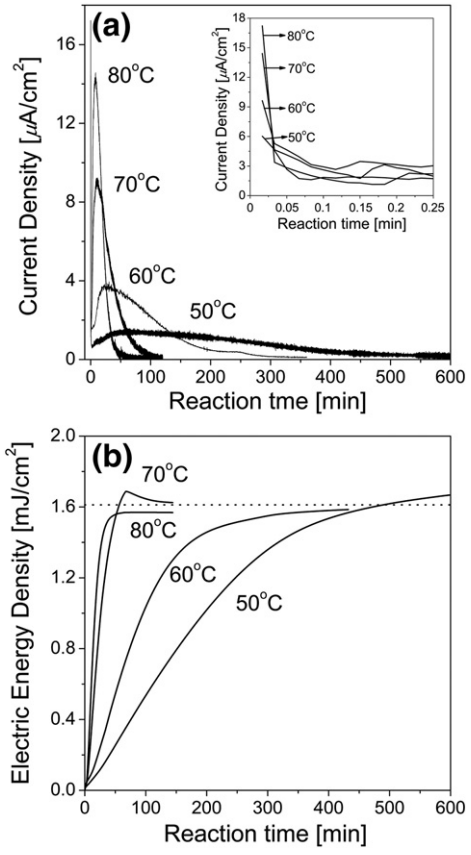

Fig. 8. (a) Current density and (b) electric energy density vs. reaction time at various temperatures during the HT–GC synthesis.

During the galvanic reactions chemical energy can be transformed into to electric energy. The output electric energy, evaluated from measured currents and voltages, as well as reaction time, is also plotted against the reaction time at various temperatures, as sketched in Fig. 8b. It shows that the electric energy increased rapidly with the reaction time and then reached a constant value that indicates the TiN surface was fully covered by $BaTiO_3$ and the galvanic reaction was self-terminated. The maximum generated electric energy density was about 1.61 ± 0.05 mJ/cm^2, which is almost independent of the reaction temperature. It is also revealed in the figure that the maximum electric energy density can be reached much faster at higher reaction temperatures, since the galvanic reactions are more enhanced at higher temperatures.

4. Conclusions

Directionally oriented (111) cubic $BaTiO_3$ films have been produced on the highly oriented (111) TiN layer by the HT–GC method above 45 °C while below 100 °C. The growth rates of $BaTiO_3$ synthesized by the HT–GC method are much faster than those prepared by the HT technique from the growth kinetic analysis. Compared to the HT methods, the HT–GC synthesis is apparently governed by more complex reaction mechanisms including the galvanic reactions. The galvanic current density was generated by the dissolution of TiN in alkaline solution and was tailored by the formation of $BaTiO_3$ over the TiN layer. The maximum galvanic current increased with the reaction temperature while the maximum current occurred at the time when

half of the TiN surface was covered by $BaTiO_3$. The output electric energy increased rapidly with the reaction time and finally leveled off at the full coverage of $BaTiO_3$. The HT–GC method with the aide of galvanic couple effects has great potentials in synthesizing many oxide materials.

Acknowledgments

The work is supported by the National Science Council of R.O.C. (Taiwan) under the grant no. NSC 98-2221-E-005-029-MY3. Thanks also to National Nano Device Laboratories (NDL) for helping in the preparation of titanium nitride films.

References

[1] R.E. Cohen, Nature 358 (1992) 136.
[2] T. Lee, I.A. Aksay, Cryst. Growth Des. 1 (2001) 401.
[3] G.H. Heartling, J. Vac. Sci. Technol. A 9 (1991) 414.
[4] H. Takahashi, Y. Numamoto, J. Tani, S. Tsuekawa, Jpn. J. Appl. Phys. 45 (2006) 7405.
[5] J. Wang, H. Wan, Q. Lin, Meas. Sci. Technol. 14 (2003) 172.
[6] M.B. Lee, M. Kawasaki, M. Yoshimoto, H. Koinuma, Appl. Phys. Lett. 66 (1995) 1331.
[7] T. Pencheva, M. Nenkov, Vacuum 48 (1997) 43.
[8] M.N. Kamalasanan, N.D. Kumar, S. Chandra, J. Appl. Phys. 76 (1994) 4603.
[9] D. Hennings, M. Klee, R. Waser, Adv. Mater. 3 (1991) 334.
[10] C. Chen, Y. Wei, X. Jiao, D. Chen, Mater. Chem. Phys. 110 (2008) 186.
[11] C.-R. Cho, E. Shi, M.-S. Jang, S.-Y. Jeong, S.-C. Kim, Jpn. J. Appl. Phys. 33 (1994) 4984.
[12] R.R. Bacsa, J.P. Dougherty, L.J. Pilone, Appl. Phys. Lett. 63 (1993) 1053.
[13] A.T. Chien, L. Zhao, M. Colic, J.S. Speck, F.F. Lange, J. Mater. Res. 13 (1998) 649.
[14] E.B. Slamovich, I.A. Aksay, J. Am. Ceram. Soc. 79 (1996) 239.
[15] C.K. Tan, G.K.L. Goh, D.Z. Chi, A.C.W. Lu, B.K. Lok, J. Electroceram. 16 (2006) 581.
[16] C.K. Tan, G.K.L. Goh, Thin Solid Films 515 (2007) 6572.
[17] S. Venigalla, P. Bendale, J.H. Adair, J. Electrochem. Soc. 142 (1995) 2101.
[18] J. Tamaki, G.K.L. Goh, F.F. Lange, J. Mater. Res. 15 (2000) 2583.
[19] P. Bendale, S. Venigalla, J.R. Ambrose, E.D. Verink Jr., J.H. Adair, J. Am. Ceram. Soc. 76 (1993) 2619.
[20] Z. Wu, M. Yoshimura, Solid State Ionics 122 (1999) 161.
[21] M. Yoshimura, S.E. Yoo, M. Hayashi, N. Ishizawa, Jpn. Appl. Phys. 28 (1989) L2007.
[22] K. Kajiyoshi, M. Yoshimura, Y. Hamaji, K. Tomono, T. Kasanami, J. Mater. Res. 11 (1996) 169.
[23] S. Agarwal, G.L. Sharma, Sens. Actuators 85 (2002) 205.
[24] T. Vargas, H. Díaz, J. Am. Ceram. Soc. 80 (1997) 213.
[25] K. Kajiyoshi, Y. Sakabe, M. Yoshimura, Jpn. J. Appl. Phys. 36 (1997) 1209.
[26] Y.-C. Chieh, C.-C. Yu, F.-H. Lu, Appl. Phys. Lett. 90 (2007) 032904.
[27] P.-H. Chan, F.-H. Lu, Thin Solid Films 517 (2009) 4782.
[28] P.-H. Chan, F.-H. Lu, J. Electrochem. Soc. 157 (2010) G130.
[29] R. Bacsa, P.R. Dranathan, J.P. Dougherty, J. Mater. Res. 7 (1992) 423.
[30] S.-B. Cho, J.-S. Noh, D.-Y. Lim, S.-H. Hong, R.E. Riman, Mater. Lett. 57 (2003) 4302.
[31] E. Shi, C.R. Cho, M.S. Jang, S.Y. Jeong, H.J. Kim, J. Mater. Res. 9 (1994) 2914.
[32] C.R. Cho, M.S. Jang, S.Y. Jeong, S.J. Lee, B.M. Lim, Mater. Lett. 23 (1995) 203.
[33] R.I. Walton, F. Millange, R.I. Smith, T.C. Hansen, D. O'Hare, J. Am. Chem. Soc. 123 (2001) 12547.
[34] J.O. Eckert Jr., C.C.H. Houston, B.L. Gersten, M.M. Lencka, R.E. Riman, J. Am. Ceram. Soc. 79 (1996) 2929.
[35] PDF-2 CDROM, International Center for Diffraction Data, Newtown Square, PA, 2000.
[36] C.-J. Yang, L.-S. Chao, F.-H. Lu, Surf. Coat. Technol. (2012), http://dx.doi.org/10.1016/j.surfcoat.2012.01.029.
[37] M. Avrami, J. Chem. Phys. 7 (1939) 1103.
[38] M. Avrami, J. Chem. Phys. 8 (1940) 212.
[39] M. Avrami, J. Chem. Phys. 9 (1941) 177.
[40] B.V. Erofe'ev, C. R. (Dokl.) Acad. Sci. L'URSS 52 (1946) 511.
[41] B.J. Kooi, Phys. Rev. B 73 (2006) 54103.
[42] H. Saitoh, A. Machida, Y. Katayama, K. Aoki, Appl. Phys. Lett. 94 (2009) 151915.
[43] R.J. Francis, S. O'brien, A.M. Fogg, P.S. Halasyamani, D. O'Hare, T. Louiseau, G. Ferey, J. Am. Chem. Soc. 121 (1999) 1002.
[44] W. Xu, L. Zheng, H. Xin, C. Lin, M. Okuyama, J. Electrochem. Soc. 143 (1996) 1133.
[45] M.E. Pilleux, V.M. Fuenzalida, J. Appl. Phys. 74 (1993) 4664.
[46] W.P. Xu, L. Zheng, C. Lin, Philos. Mag. B 77 (1998) 177.
[47] W.P. Xu, L. Zheng, H. Xin, C. Lin, M. Okuyama, J. Mater. Res. 11 (1996) 821.
[48] C.F. Windisch Jr., J.W. Virden, S.H. Elder, J. Liu, M.H. Engelhard, J. Electrochem. Soc. 145 (1998) 1211.
[49] A.J. Bard, L.R. Faulkner, Electrochemical Methods, Wiley Interscience, New York, 2001.